



Effect of humidity on the evolution of COVID-19 droplets distribution in extreme in-homogeneous environment

CHANDRA SHEKHAR PANT^{1,*} and SACHIDANANDA BEHERA²

¹Faculty of Mechanical Engineering, Technion-Israel Institute of Technology, Haifa, Israel

²Department of Mechanical Engineering, Indian Institute of Technology Bombay, Bombay, India
e-mail: chandukec@gmail.com

MS received 16 February 2021; revised 15 June 2021; accepted 12 August 2021

Abstract. We numerically modeled the droplets' size distribution of sneezing action from the COVID-19 patient, without considering the viral loading of droplets. Thus, we assumed the behavior of COVID-19 droplets same as that of *standard water droplets*. In this work, we evolved the initial Weibull distribution (typically used for representing the saliva droplets size distribution) using a non-dimensional droplet size distribution equation under extreme in-homogeneous conditions. We varied the environmental humidity contrast according to the range primarily encountered in the world's major cities. We found bimodal size distribution of droplets for every humidity contrast, previously reported to be a function of Stoke's number. This bimodal size distribution of droplets is a consistent event in in-homogeneous mixing. The high humidity contrast between the sneezing zone of influence to the environment will have a comparatively long tail of droplets. This long tail of droplets implies that the evaporation time scales will be highly variable and, consequently, significantly impact the transmission of the virus from a COVID-19 patient to a healthy human being. Essentially means that these cities of high humidity contrast will be more prone to high infections.

Keywords. COVID-19; droplet size distribution; inhomogeneous mixing; environmental humidity.

1. Introduction

COVID-19 has been declared as a pandemic, claiming 1 million deaths to date and still counting. On July 9th, 2020, WHO said that "airborne transmission" of COVID-19 in poorly ventilated locations "cannot be ruled out" [1]. Also, Morawska and Cao [2] emphasized the importance of airborne transmission of COVID-19. While sneezing, the infected person's droplets can travel over a region of "influence" or could be suspended in the atmosphere, which eventually could transmit the virus (by transporting droplets) to the neighboring fellow. Thus, this sneezing phenomenon is a vital aspect to consider while framing the overall policy regarding public transport and public gathering.

While sneezing, broad size spectra of droplets are being ejected; it could be tiny droplets of the range of a few microns or size in hundreds of microns [3–9]. The flow behavior of the smaller droplets is primarily governed by the microscopic phenomena like Kelvin and Köhler effects. Consequently, the "likelihood" of the COVID-19 virus depends on these phenomena. This aspect of the "likelihood of survival of coronavirus" was extensively studied by Bhardwaj and Agrawal [4, 10]. But, as expected, the

larger droplets' behavior will be influenced by inertia and gravity. The combined effects of these factors were studied in the work of Munir and Xu [11]. In this work, they found that gravity and surface tension plays an important role in propagating the micro-bubble. In addition to the "likelihood" of the coronavirus, the other aspect that has to be taken into account is the distance traveled by these droplets in the ambient surrounding before the droplets get dissipated in the environment [12, 13]. Concerning this point, Cummins *et al* [14] using the analytical model, deduced that the intermediate size droplets achieve the minimum horizontal range. Also, they argued that the "bi-modal" distribution of droplet size is a function of the Stokes number. In a similar context, Das *et al* [15] using Monte-Carlo simulations demonstrated that the bigger droplets travel a considerable distance. However, the smaller droplets remain suspended for a longer time and thus concluded that spatial and temporal isolation is vital for preventing the virus's spread. Meanwhile, Vadivukkarasan *et al* [16], through rigorous experiments, concluded that the size distribution of droplets coming out of the respiratory fluids depends on the multiple hydrodynamic instabilities. Furthermore, they pointed out that aerosol generation could be attributed to these instabilities. Interestingly, Prasanna Simha and Mohan Rao [17] using experimental analysis found a universal exponential decaying distance-velocity

*For correspondence

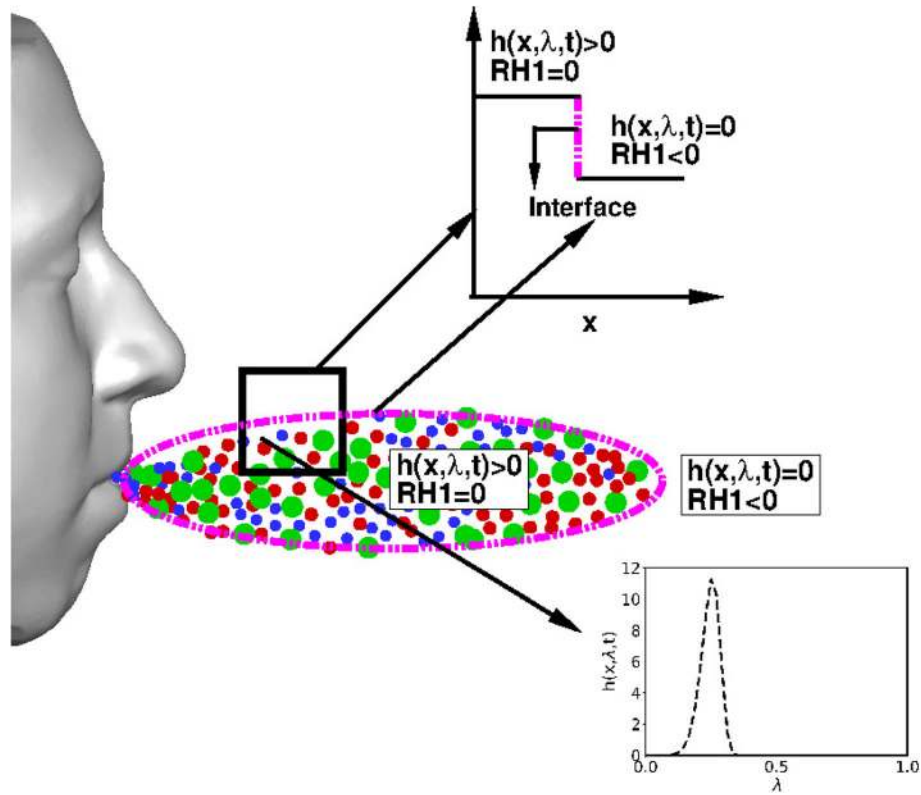


Figure 1. Schematic of the problem set up. The square box is the area of interest in which a step function for the variables is assumed. The interface between the sneezing and non-sneezing zone is depicted by the dash-dotted purple line. The standard triangular file (STL) of the human face is taken from [38].

law in the human coughing flow dynamics. They argued that the viscous vortex rings govern this universal flow dynamics pattern. On the preventive aspect from the COVID-19, Dbouk and Drikakis [18] demonstrated the effectiveness of the masks to prevent the spread of the virus through droplets. In addition to this seminal article, in a separate work, they studied the weather conditions on the spread of the droplets [19]. They pointed out that the local weather conditions, primarily the humidity and temperature, will play a decisive role in the second wave of the COVID-19 pandemic. Pendar and Páscoa [20] numerically investigated different scenarios of sneezing and coughing and found that the shorter people are more prone to get affected by the virus because of the droplet’s trajectory coming out from the sneezing/coughing person.

The flow dynamics associated with the sneezing and/or coughing was modeled or visualized as a free shear flow such as turbulent jet/plume [21–25]. While modeling the flow as a jet with the volumetric heating, the flow dynamics is affected by the initial buoyancy; this effect was numerically studied and modeled by Pant and Bhattacharya [26] and Bhattacharya and Pant [27]. Similarly, cumulus clouds were represented as turbulent jets/plumes [28–31]. Considering the same modeling analogy, we are trying to

incorporate the idea of cloud microphysics in the event of human sneezing. Also, recently, Diwan *et al* [32] in the section “Two closely related fluid flow problems” postulated that “cumulus cloud flows” and “dynamics of small water droplets” are “relevant flow problems” to understand the coughing/sneezing actions. Thus, the present work is motivated to import the present understanding of the mixing in clouds to interpret and expand the understanding of sneezing under the extreme scenario of in-homogeneous mixing. Although we sincerely acknowledge that these two fields (human sneezing and cloud) are entirely different with respect to scale, Reynolds number, and physical/biological perspectives. In clouds, the mixing is primarily divided into two main types: homogeneous and in-homogeneous mixing. Mathematically quantified as Damköhler number(Da), given by:

$$Da = \frac{\tau_F}{\tau_D} \tag{1}$$

here, τ_F is the mixing/fluid time scale and τ_D is the time scale associated for droplets [33, 34]. Depending on the problem scenario, τ_D is either referred to as phase relaxation time of droplets or the evaporation time scale of droplets [34]. When the time scale of mixing/fluid (τ_F) is

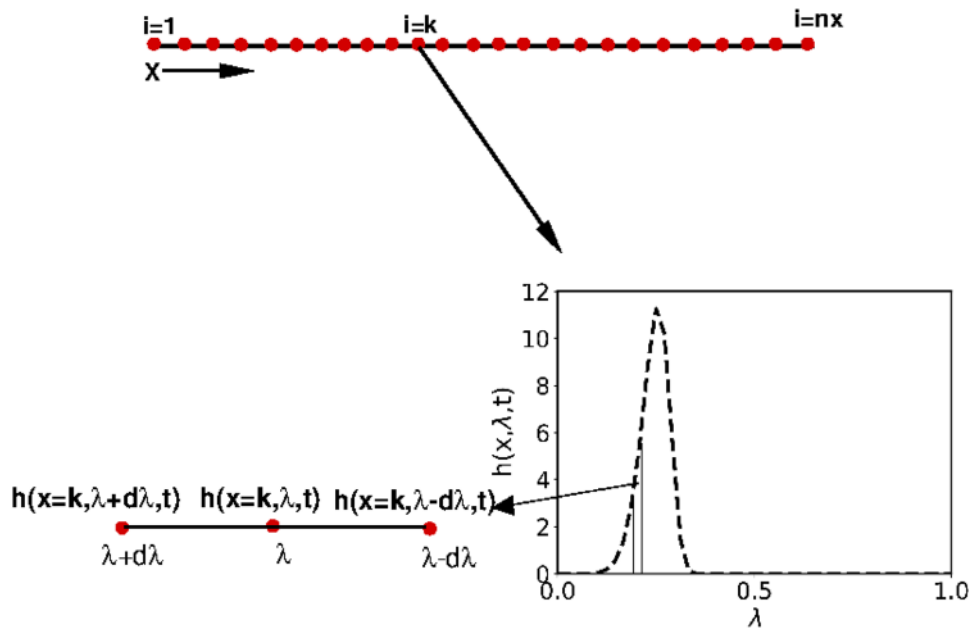


Figure 2. Methodology: A straight horizontal line represents a one-dimensional domain, red dots showing the grid points, initially at each grid nodes the DSD is defined, and this DSD is divided into bins of length $d\lambda$.

much less than the evaporation time scale of droplets ($Da \ll 1$), the mixing is referred to as homogeneous mixing. It can be physically interpreted as the scenario when the in-homogeneities in the domain are well mixed before the droplet’s response. On the other hand, when the time scale of mixing/fluid (τ_F) is much larger than the evaporation time scale of droplets ($Da \gg 1$), the mixing is referred to as in-homogeneous mixing. This situation can be physically understood as the immediate response of droplets via evaporation/condensation to the in-homogeneous domain before the inhomogeneities are well mixed by the fluid mixing scales. The droplets tend to evaporate in a few seconds (depending on the size) [24]; thus, the mixing at the sneezing interface can be regarded as a case of extreme in-homogeneous mixing.

Srivastava [35] reported an extensive survey to demonstrate an interplay between the COVID-19 virus transmission and various atmospheric parameters viz. temperature, humidity, wind speed, and the particulate matter. He emphasized that a direct correlation exists between the particulate/gaseous pollutant and the COVID-19 cases. Furthermore, he noted that humidity/temperature has an inverse effect on the COVID-19 transmission. However, in the works of [4, 19, 36] they showed that with the increasing humidity level of the environment, the possibility of the COVID-19 survival increases. Thus, the present work focuses on the effect of humidity contrast between the sneezing zone of the COVID-19 patient and the ambient environment. The initial size distribution of the saliva droplets exhaled during talking/coughing is assumed to follow Weibull distribution [8, 37]. Furthermore, we

assumed no distinction between the (COVID-19) virus-laden droplet distribution and the normal coughing/sneezing distribution. Specifically, categorization of droplet distribution according to the higher or lower viral loadings is beyond the scope of the present work.

2. Problem set up, governing equations, methodology and initial condition

2.1 Problem set up

We are considering a 1-D domain ($0 \leq x \leq 1$) in which step function of the variables is considered. Figure 1 shows the schematic of the problem set-up. We assume that the COVID-19 droplets’ sneezing has a domain of influence represented by the dotted purple line. This purple line distinguishes the sneezing (domain of influence, $0 \leq x < 0.5$) region from the surrounding atmosphere ($0.5 \leq x \leq 1$). This sneezing region ($0 \leq x < 0.5$) contains droplets of the COVID-19 virus and has saturated humidity. In contrast, the surrounding atmosphere ($0.5 \leq x \leq 1$) is devoid of these droplets and has humidity based on the city’s location. We took a section of this phenomenon (square box in the figure 1) and modeled it as a 1-D problem ($0 \leq x \leq 1$). Thus, overall the region $0 \leq x < 0.5$ represents the domain of influence for the sneezing action while region $0.5 \leq x \leq 1$ signifies an ambient condition driven by the humidity of the environment. The size distribution of the COVID-19 droplets is assumed as the Weibull distribution, which is given by the equation 2:

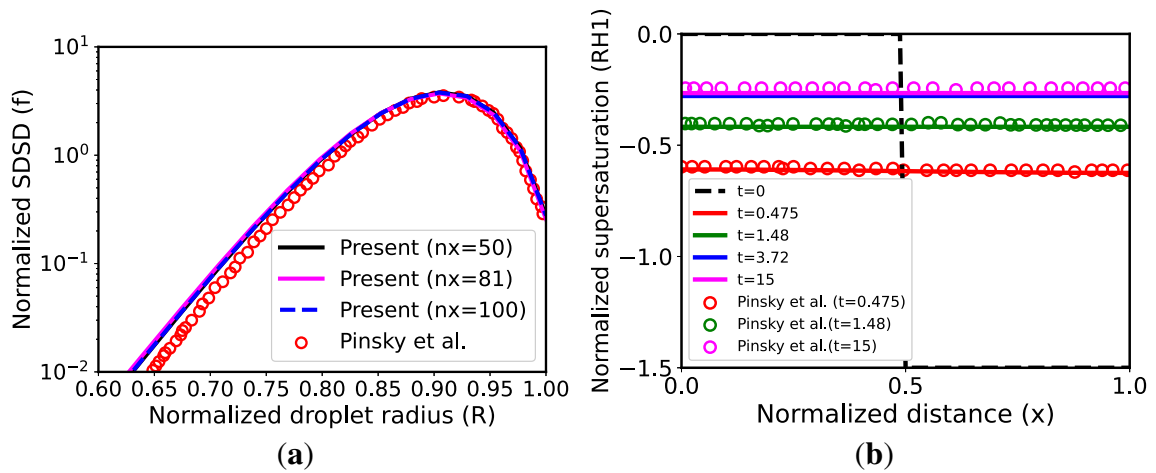


Figure 3. Validation against the work of Pinsky *et al* [40] for (a) normalized standard droplet size distribution (SDSD), corresponds to the figure 6(b) in Pinsky *et al* [40] and (b) normalized relative humidity (RH1), referred as normalized supersaturation in Pinsky *et al* [40], referred as figure 3(a) in Pinsky *et al* [40].

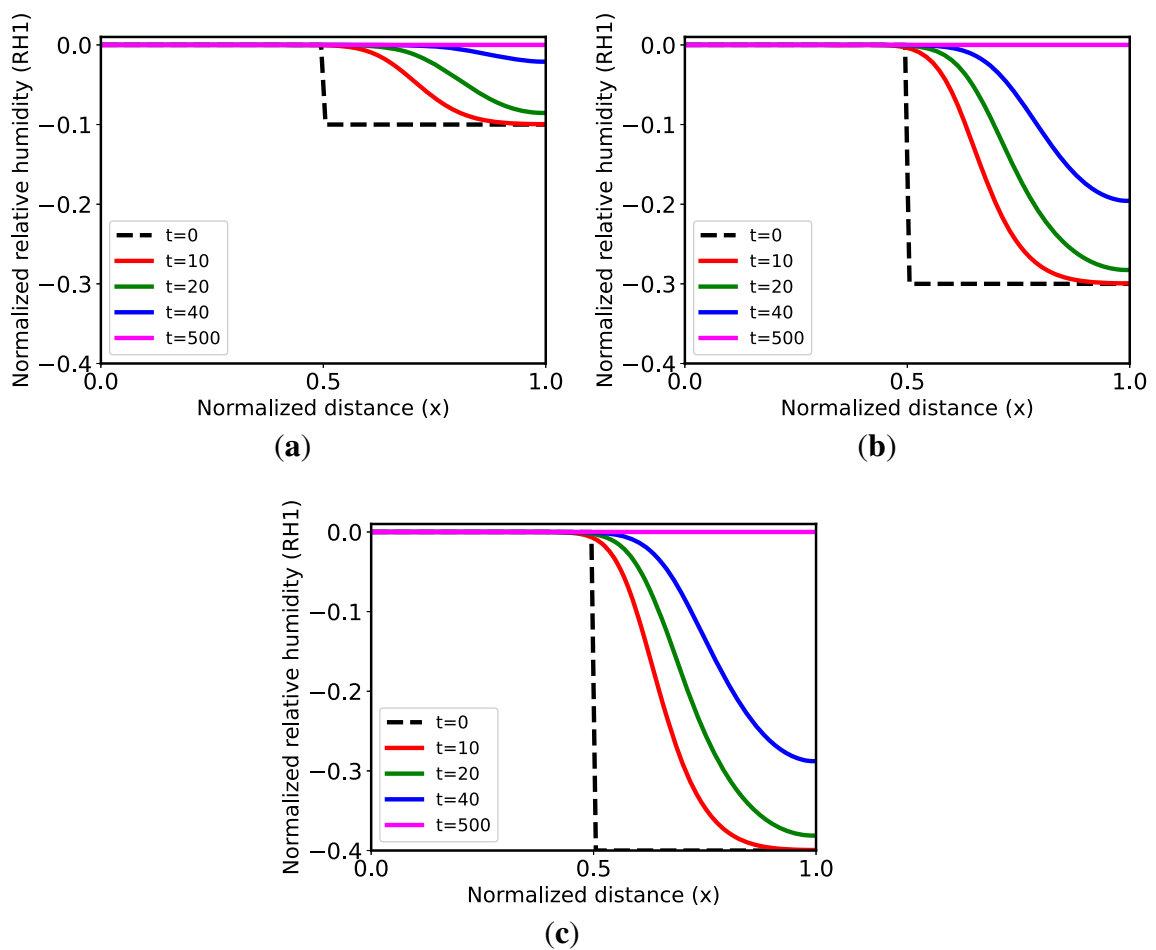


Figure 4. Variation of normalized relative humidity (RH1) with respect to time for initially (a) $RH2 = -0.1$ (b) $RH2 = -0.3$ and (c) $RH2 = -0.4$.

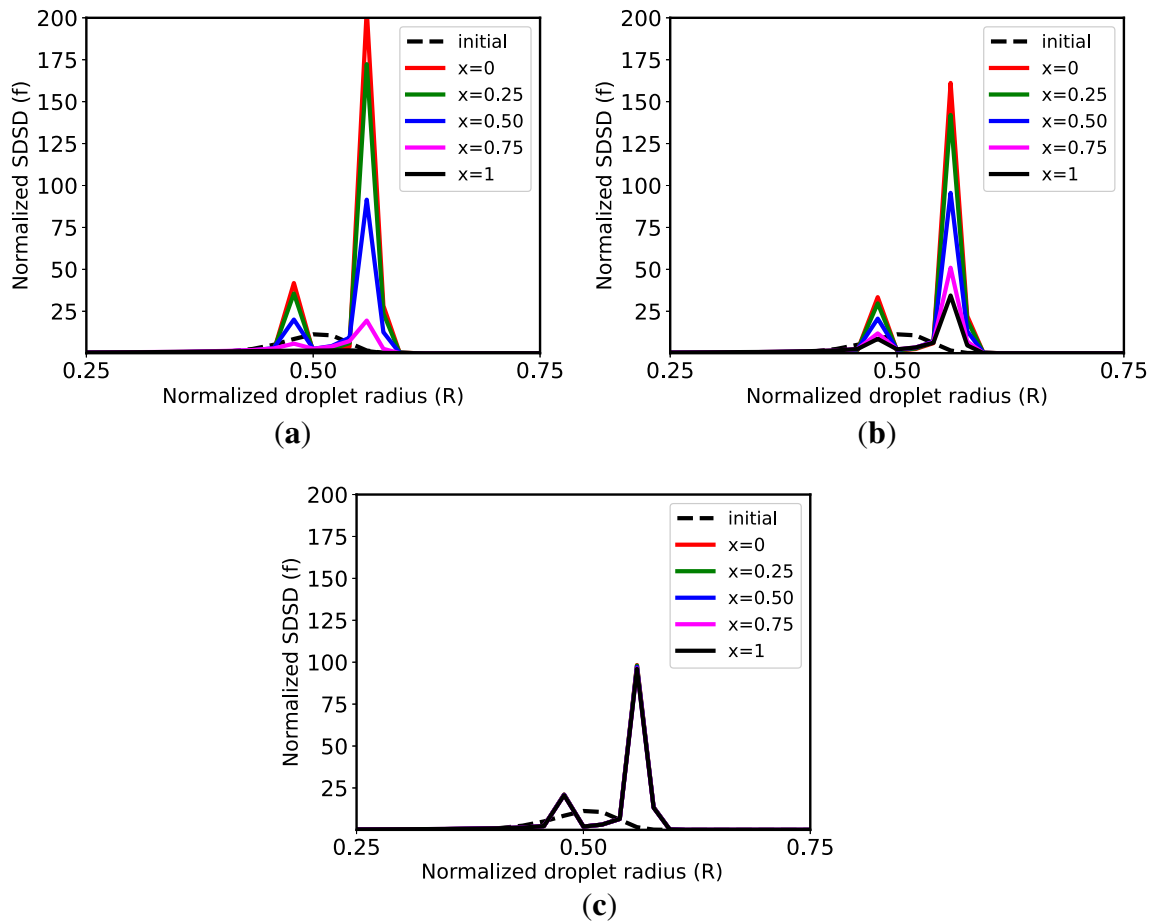


Figure 5. Variation of SDS for case $RH2 = -0.1$ against time at (a) $t = 50$, (b) $t = 100$ and (c) $t = 500$.

$$h = \frac{n}{\lambda_p} \left(\frac{\lambda}{\lambda_p} \right)^{n-1} e^{-(\lambda/\lambda_p)^n} \tag{2}$$

here, $n = 8$, $\lambda_p = 0.26$, and λ is normalized radius square described in section 2.2. These values of n and λ_p are considered from the work of Dbouk and Drikakis [37]. Noting that the value of λ_p is scaled in the range of $[0, 1]$. This size distribution of droplet is shown in figures 1 and 2. Dbouk and Drikakis [37] emphasized that, while coughing, the droplets size distribution is best fitted with the Rosin–Rammler or Weibull distribution. While modeling this simplified problem set up, we assumed that the growth of the droplets is governed by one-dimensional diffusion of vapor, thus neglecting the droplet collision. We are neglecting the surface effects, primarily known as Kelvin and Köhler effects. We assume that the Stokes’ number is relatively small, thus neglecting the sedimentation effects. Furthermore, we are also ignoring the fluid/flow properties change due to the presence of mucus during sneezing. In this work, we are making a further assumption of adiabatic mixing, which implies that the effect of temperature is neglected. A similar set-up of the

problem was previously used in a two-dimensional framework by Pant and Bhattacharya [39] and in one-dimensional scope by Pinsky *et al* [40] from the perspective of clouds.

2.2 Governing equations and methodology

We solved the following governing equations in a one dimensional frame-work. These set of equations are primarily mimicking the evaporation and diffusion growth of droplets [40]. Pinsky *et al* [40] have derived and used these equations to understand, explain and formulate the inhomogeneous mixing in clouds.

$$q(x, t) = \int_0^\infty \lambda^{3/2} h(x, t, \lambda) d\lambda \tag{3}$$

$$\frac{\partial \Gamma(x, t)}{\partial t} = \frac{1}{Da} \frac{\partial^2 \Gamma(x, t)}{\partial x^2} \tag{4}$$

$$RH1(x, t) = \Gamma(x, t) - q(x, t) \tag{5}$$

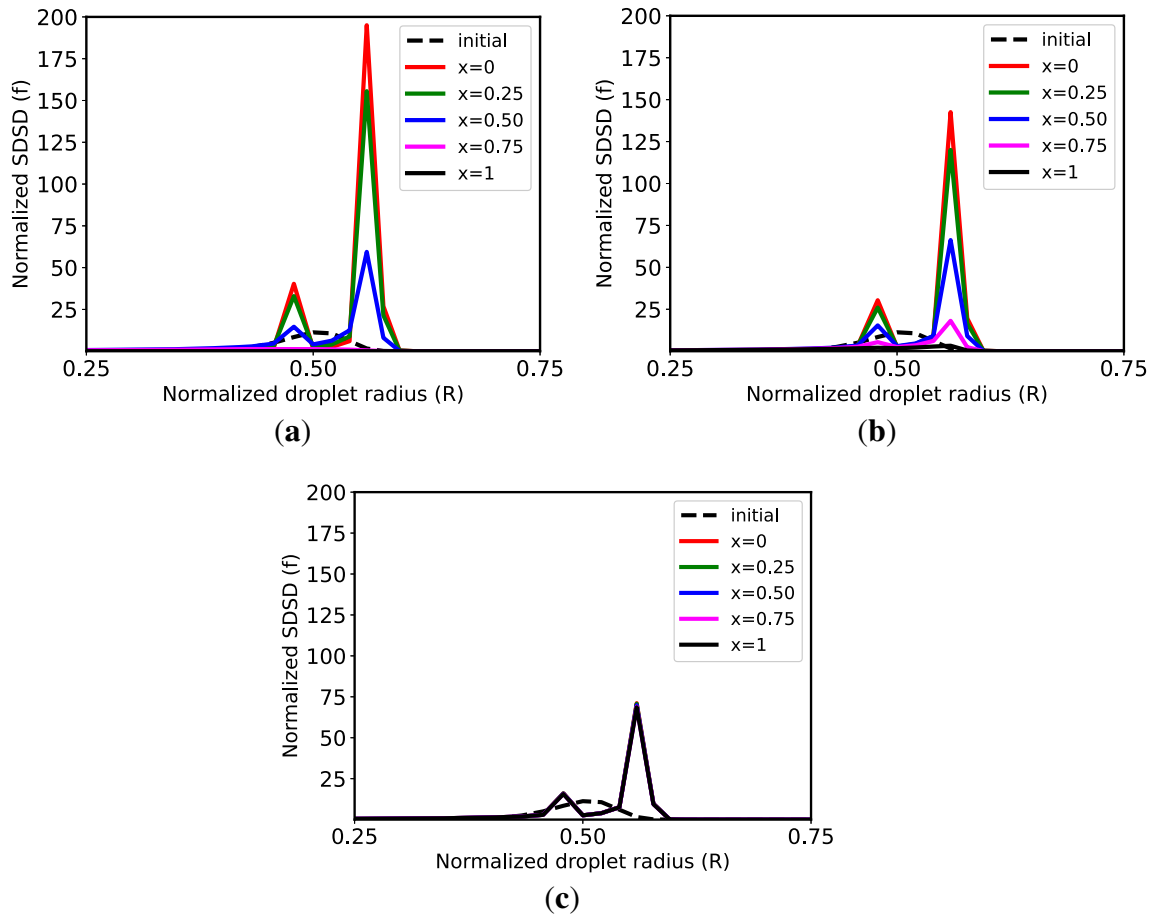


Figure 6. Variation of SDS for case RH2 = −0.3 against time at (a) t = 50, (b) t = 100 and (c) t = 500.

$$\frac{\partial h(x, t, \lambda)}{\partial t} = \frac{1}{Da} \frac{\partial^2 h(x, t, \lambda)}{\partial x^2} - \frac{2}{3} (RH1(x, t)) \frac{\partial h(x, t, \lambda)}{\partial \lambda} \quad (6)$$

$$\lambda = R^2 \quad (7)$$

here, R is radius. Eqn 3 signifies the liquid water ratio ($q(x, t)$) that is contained inside the droplets. $\Gamma(x, t)$ is a conservative variable governed by the Eqn 4. From these two variables ($q(x, t)$ and $\Gamma(x, t)$), the RH1(x,t) (named as normalized supersaturation in Pinsky *et al* [40]) referred as normalized relative humidity is computed using Eqn 5. Finally, the evolution of droplets size distribution $h(x, t, \lambda)$ is governed by Eqn 6. The first term on the right-hand side of the Eqn 6 relates to the diffusion, while the second term relates to the evaporation phenomena. Thus, the DSD is governed by the dual effect of inhomogeneity inside the domain and the droplets’ evaporation due to the humidity contrast. To be noted here that the DSD $h(x, \lambda, t)$ is a function of spatial coordinates (x) and droplets radius ($\lambda = R^2$). The extent of “mixing” or “flow behavior” is governed by the parameter Damköhler number(Da). Under the assumption of quiescent environment the time travel of

sneezing is approximately 22 s [41], thus for the droplets of diameter (2 – 3 μm) the typical value of $Da \sim 22/1 \sim 22$. In the present work, we consider the COVID-19 droplets distribution in a scenario of extreme in-homogeneous mixing ($Da = 1000$), with different humidity levels. This value of Damköhler number ($Da = 1000$) is chosen to emphasize that the response of COVID-19 droplets in the ambient surrounding will be relatively much faster as compared to the environmental mixing time scales. However, this specific value of 1000 is considered heuristically to signify that the Damköhler number is comparatively very high than 1 to be safely regarded as inhomogeneous mixing. While considering the $Da = 1000$ we assume that from small droplets (less than 1 μm) the evaporation time scale if 0.02 s and thus the value of Damköhler number (Da) is given by:

$$Da = \frac{\tau_F}{\tau_D} = \frac{22}{0.022} = 1000 \quad (8)$$

While the influence of ambient conditions is tuned by the term RH1. All these equations are written in the normalized

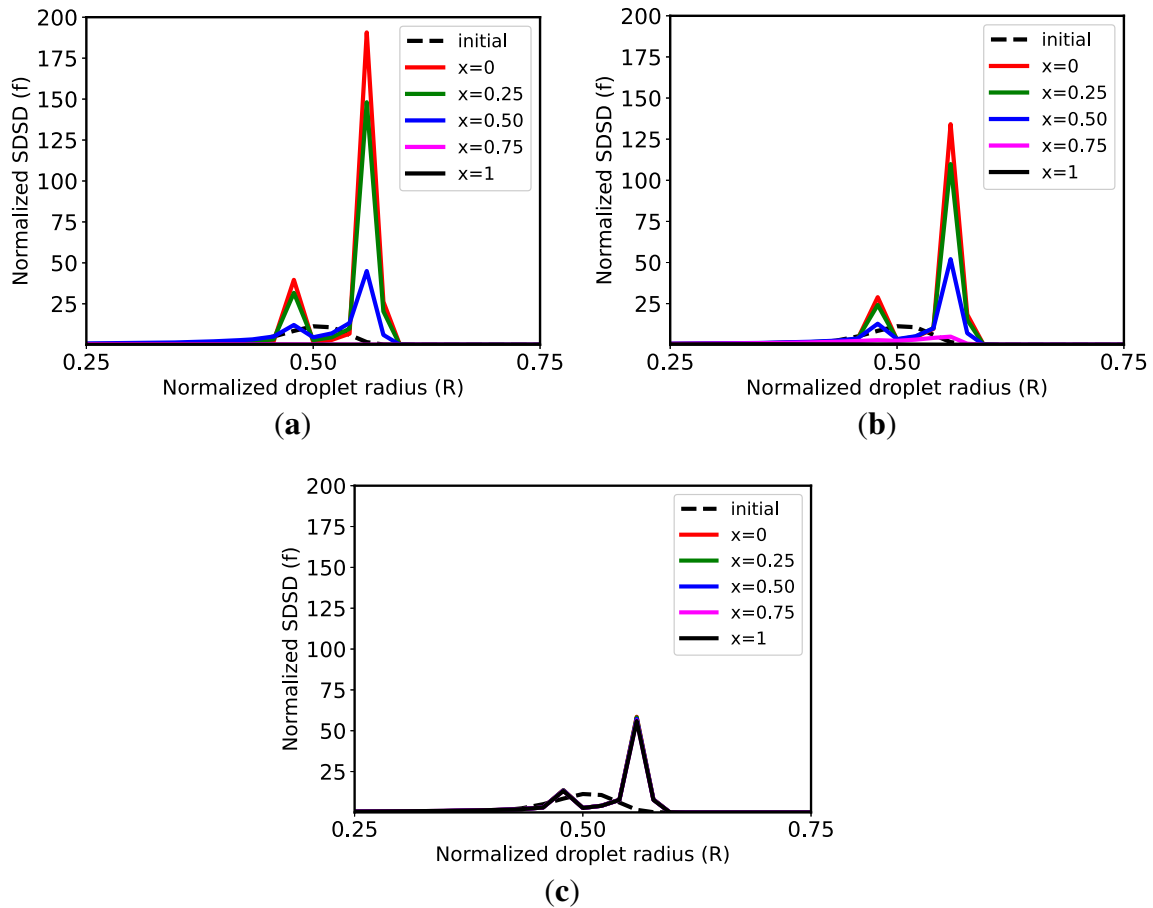


Figure 7. Variation of SDS for case RH2 = −0.4 against time at (a) t = 50, (b) t = 100 and (c) t = 500.

form; for further details, refer to Pinsky *et al* [40]. Figure 2 shows the methodology of the finite difference method used to solve these set of coupled equations. The length of the domain is 1, and it is discretized into grid points (total points = nx); at each grid point, the DSD is defined. The DSD is considered according to the Eqn 2 and plotted in figure 2. This DSD at each grid nodes is discretized into bins of $d\lambda$ divisions (total divisions = np). Standard central differencing scheme (CDS) is used to discretize the second-order terms while first-order Euler time stepping is used for time marching. The time step is less than the diffusion time scale for each case.

2.3 Initial conditions

The initial conditions for the $\Gamma(x, t)$ and $h(x, \lambda, t)$ (DSD) are defined as step function and mathematically given by:

$$\Gamma(x, 0) = \begin{cases} 1 & \text{if } 0 \leq x < 0.5 \\ RH2 & \text{if } 0.5 \leq x \leq 1 \end{cases} \quad (9)$$

$$h(x, \lambda, 0) = \begin{cases} \frac{n}{\lambda_p} \left(\frac{\lambda}{\lambda_p}\right)^{n-1} e^{-(\lambda/\lambda_p)^n} & \text{if } 0 \leq x < 0.5 \\ 0 & \text{if } 0.5 \leq x \leq 1 \end{cases} \quad (10)$$

Noting that the 1D domain is spanning as $0 \leq x \leq 1$. In the present work we are defining the RH2 = RH − 1 and varying the value of RH2 as −0.1, −0.3 and −0.4. These RH values (varying from 60% to 90%) corresponds to the ambient humidity level taken from the online data for the month of August for 6 major cities (viz. Beijing, Mumbai, New York, Sydney, Singapore and London) [42]. Specifically we considered the relative humidity RH = 90%, 70% and 60%.

3. Validation and grid independence study

For validation purpose, we considered a similar setup described in Pinsky *et al* [40], in which the mono-dispersed DSD was considered, $Da = 1$ and RH2 was fixed at −1.5. The number of bins for the DSD discretization is fixed at $np = 24$. Figure 3 shows the comparison of the present

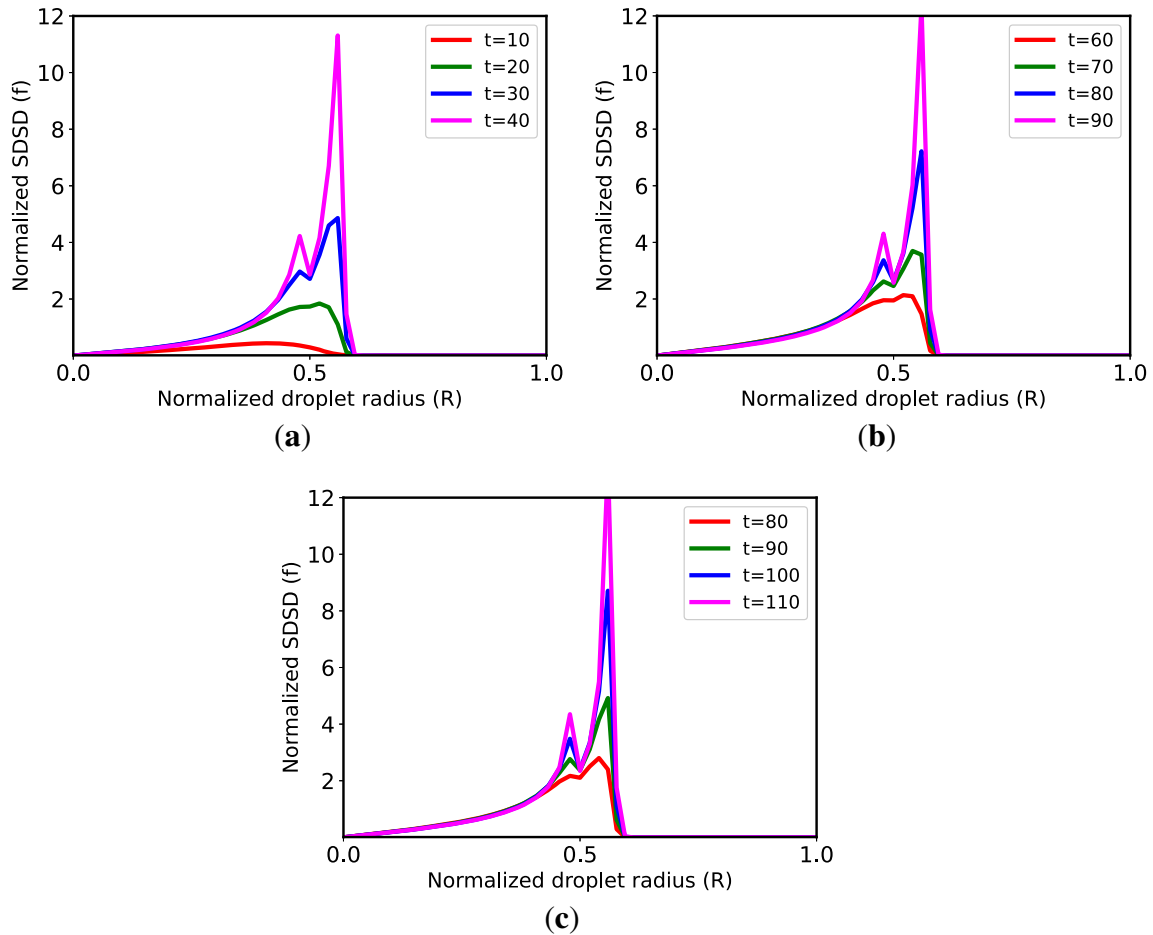


Figure 8. Variation of SDSD at $x = 0.75$ for (a) $RH2 = -0.1$, (b) $RH2 = -0.3$ and (c) $RH2 = -0.4$.

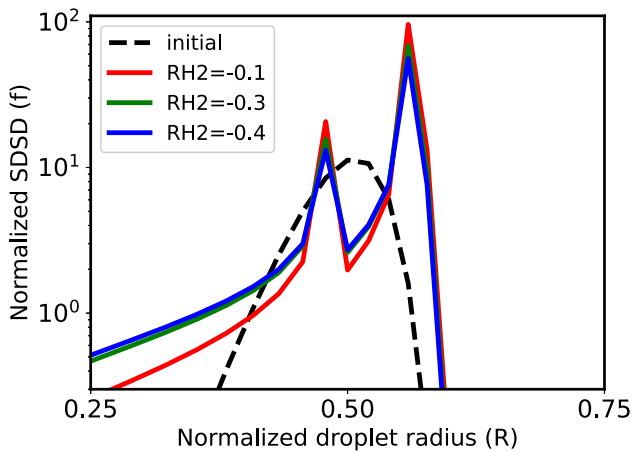


Figure 9. Comparison of final (at $t = 500$) SDSD (in log scale) for all the humidity contrast.

work against the previous work of [40]. Figure 3(a) compares the normalized droplet size distribution (named as SDSD) at $t=0.475$. Here we are representing SDSD by $f(x, R, t)$ and this quantity is related to DSD ($h(x, t, \lambda)$) by Eqn 11

$$f(x, R, t) = 2R \times h(x, \lambda, t) \tag{11}$$

The present work matches well with the previous work of Pinsky *et al* [40]. Also, we compared the SDSD for different resolutions ($nx = 50, 81, 100$) to check our results' sensitivity with the grid size and found that the results are independent of the grid resolutions. In the rest of the manuscript we have simulations corresponding to $nx = 100$ and $np = 50$. Similarly, in figure 3(b), we are comparing the variation of normalized supersaturation (RH1) of present work against the previous work of Pinsky *et al* [40]. Pinsky *et al* [40] solved the governing equations using “PDEPE” utility of MATLAB. Thus, difference between the present and the prior work of Pinsky *et al* [40] could be because of the different methodologies for solving the governing equations.

4. Results and discussions

In this section, we first consider the variation of humidity with time in the domain. Figure 4(a) shows the variation of normalized humidity (RH1) with respect to time for the

lowest humidity contrast case ($RH2 = -0.1$). From hereon, for simplicity, we are denoting the normalized humidity ($RH1$) as humidity. Please note that in sections 2.2 and 2.3, we are representing $RH2$ as normalized initial humidity, $RH1$ as normalized relative humidity, and RH as normalized ambient relative humidity. With the passage of time, the humidity contrast between the two sections of the domain decreases and finally attains the complete saturation state. While comparing the different initial humidity contrast (figures 4(b) and 4(c)), the time to completely homogenize the humidity level increases with the increase in the humidity contrast. This can be understood by the difference in the initial humidity level; because of the high humidity contrast, the mixing took a long time to homogenize the humidity in the domain. The final saturation state ($RH1 = 0$) for all the cases signifies that some droplets have completely evaporated and have liberated the water vapor and consequently have saturated the domain in the process of mixing the gradients. This phenomenon will be explained in the next paragraph.

Figures 5–7 shows the evolution of normalized standard droplet size distribution (SDSD) against time for different humidity contrast case ($RH2 = -0.1$, $RH2 = -0.3$ and $RH2 = -0.4$). In these figures, two sections ($x = 0$ and $x = 0.25$) are considered inside the saturation section, while the other two sections are considered in the saturation deficit region ($x = 0.75$ and $x = 1$), and a section at the interface ($x = 0.5$) is considered. Initially at $t = 50$, shown in figure 5(a) the droplets in the saturated zone ($x = 0$) have evolved in the “bi-modal” distribution which is an important aspect of inhomogeneous mixing [43, 44]. Also, the “bi-modal” distribution of droplet size while sneezing was reported in the experiments of Han *et al* [3]. They attributed this distribution to biological phenomena. But, recently, the analytical work of Cummins *et al* [14] credited this distribution as the consequence of droplets’ Stokes number. This “bi-modal” distribution have taller peaks for larger radius and smaller peaks related to a smaller radius. This implies that most droplets grew larger (because of condensation), while a smaller number of droplets have undergone evaporation. A similar trend is followed at $x = 0.25$, while important phenomena occur in the humidity deficit region. To emphasize it, we are considering the growth of the droplets at $x = 0.75$ section of the domain since the SDSD looks similar for all the humidity contrast in the regions of $x = 0$ and $x = 0.5$ or in the saturated regions. This is not surprising since, at these locations, the initial conditions were the same.

Figure 8(a) shows the evolution of SDSD with respect to time in the humid deficit region (at $x = 0.75$) for the $RH2 = -0.1$ case. Initially (at $t = 10$), the droplets evaporate, and thus, the SDSD widens corresponding to the smaller droplets. The evaporation of droplets liberate vapor in the domain, hindering the other droplets from undergoing evaporation, and in fact, experienced condensational growth. Thus, there is simultaneous evaporation and condensation of droplets, resulting in the “bi-modal”

distribution (at $t = 30$ and $t = 40$). The similar pattern is also evident for the higher humidity contrast cases ($RH2 = -0.3$ and $RH2 = -0.4$), shown in figures 8(b) and 8(c). But, the number of completely evaporated droplets are higher for the higher humidity contrast case. Certainly, because of these evaporated droplets, the final SDSD for different humidity contrast also varies and will be discussed in the next paragraph.

On comparing the final SDSD for all the humidity ratio (shown in figure 9), we found that the asymmetric bimodal size distribution is a consistent feature in all the humidity contrast. Asymmetry in the size distribution is due to the fact that large portion of droplets keep growing because of condensational growth while a smaller portion of droplets are evaporated to make the 1D parcel/box saturated. A long-tail corresponding to the smaller radius signifies the droplets’ evaporation for all the humidity cases. Simultaneously, droplets are also prone for condensational growth; this tendency will be highest when the humidity contrast is minimal ($RH2 = -0.1$). Now, since the droplets have very large spectra of size distribution, i.e., from very small size to very large size droplets, their time scales of evaporation also vary from fractions of seconds to half a second [24]. The smaller droplets tend to remain suspended in the air for a long time, while the larger droplets will travel a larger horizontal distance [15]. Therefore it can be cautiously concluded that under highly in-homogeneous conditions and with the high humidity contrast between the sneezing zone and environment, the rate of infection would be higher.

5. Conclusion

Using the simplified 1D-diffusion equation, we evolved the droplet size distribution (DSD) of COVID-19 droplets ejecting from the human sneezing under extreme in-homogeneous mixing condition with varying humidity contrast between sneezing influenced zone and the ambient environment. We found that under these conditions, a “bi-modal” distribution is evident, having a long tail of droplets with a lower radius, which signifies the evaporation of droplets. Simultaneously, droplets are prone to condensation, which increases the diameter of the droplets. This wide range of droplets diameter, in turn, will have different evaporation time scales. Consequently the smaller droplets remain suspended in the ambient atmosphere for a longer time while larger droplets travel larger horizontal distance [15]. This effectively implies that the transmissibility of COVID-19 increases for high humidity contrast region.

References

- [1] <https://www.livescience.com/who-covid-19-airborne-transmission-update.html>; accessed 02 September, 2020

- [2] Morawska L and Cao J 2020 Airborne transmission of sars-cov-2: the world should face the reality. *Environ. Int.* 105730
- [3] Han Z Y, Weng W G, and Huang Q Y 2013 Characterizations of particle size distribution of the droplets exhaled by sneeze. *J. Roy. Soc. Interface* 10: 20130560
- [4] Bhardwaj R and Agrawal A 2020 Likelihood of survival of coronavirus in a respiratory droplet deposited on a solid surface. *Phys. Fluids* 32: 061704
- [5] Wang B, Wu H, and Wan X F 2020 Transport and fate of human expiratory droplets—a modeling approach. *Phys. Fluids* 32: 083307
- [6] Yang S, Lee G W M, Chen C M, Wu C C, and Yu K P 2007 The size and concentration of droplets generated by coughing in human subjects. *J. Aerosol Med.* 20: 484–494
- [7] Chao C Y H, Wan M P, Morawska L, Johnson G R, Ristovski Z D, Hargreaves M, Mengersen K, Corbett S, Li Y, Xie X, et al. 2009 Characterization of expiration air jets and droplet size distributions immediately at the mouth opening. *J. Aerosol Sci.* 40: 122–133
- [8] Xie X, Li Y, Sun H, and Liu L 2009 Exhaled droplets due to talking and coughing. *J. R. Soc. Interface* 6: S703–S714
- [9] Asadi S, Wexler A S, Cappa C D, Barreda S, Bouvier N M, and Ristenpart W D 2019 Aerosol emission and superemission during human speech increase with voice loudness. *Sci. Rep.* 9: 1–10
- [10] Bhardwaj R and Agrawal A 2020 Tailoring surface wettability to reduce chances of infection of covid-19 by a respiratory droplet and to improve the effectiveness of personal protection equipment. *Phys. Fluids* 32: 081702
- [11] Munir B and Xu Y 2020 Effects of gravity and surface tension on steady microbubble propagation in asymmetric bifurcating airways. *Phys. Fluids* 32: 072105
- [12] Gao N and Niu J 2006 Transient CFD simulation of the respiration process and inter-person exposure assessment. *Build. Environ.* 41: 1214–1222
- [13] Zhu S, Kato S, and Yang J H 2006 Study on transport characteristics of saliva droplets produced by coughing in a calm indoor environment. *Build. Environ.* 41: 1691–1702
- [14] Cummins C P, Ajayi O J, Mehendale F V, Gabl R, and Viola I M 2020 The dispersion of spherical droplets in source–sink flows and their relevance to the covid-19 pandemic. *Phys. Fluids* 32: 083302
- [15] Das S K, Alam J, Plumari S, and Greco V 2020 Transmission of airborne virus through sneezed and coughed droplets. *Phys. Fluids* 32: 097102
- [16] Vadivukkarasan M, Dhivyaraja K, and Panchagnula M V 2020 Breakup morphology of expelled respiratory liquid: from the perspective of hydrodynamic instabilities. *Phys. Fluids* 32: 094101
- [17] Simha P P and Rao P S M 2020 Universal trends in human cough airflows at large distances. *Phys. Fluids* 32: 081905
- [18] Dbouk T and Drikakis D 2020 On respiratory droplets and face masks. *Phys. Fluids* 32: 063303
- [19] Dbouk T and Drikakis D 2020 Weather impact on airborne coronavirus survival. *Phys. Fluids* 32: 093312
- [20] Pendar M R and Páscoa J C 2020 Numerical modeling of the distribution of virus carrying saliva droplets during sneeze and cough. *Phys. Fluids* 32: 083305
- [21] Bourouiba L, Dehandschoewercker E, and Bush J W M 2014 Violent expiratory events: on coughing and sneezing. *J. Fluid Mech.* 745: 537–563
- [22] Busco G, Yang S R, Seo J, and Hassan Y A 2020 Sneezing and asymptomatic virus transmission. *Phys. Fluids* 32: 073309
- [23] Mittal R, Ni R, and Seo J H 2020 The flow physics of covid-19. *J. Fluid Mech.* 894: F2-1.
- [24] Chaudhuri S, Basu S, Kabi P, Unni V R, and Saha A 2020 Modeling the role of respiratory droplets in covid-19 type pandemics. *Phys. Fluids* 32: 063309.
- [25] Gupta J K, Lin C H, and Chen Q 2009 Flow dynamics and characterization of a cough. *Indoor air* 19: 517–525
- [26] Pant C S and Bhattacharya A 2018 Evaluation of an energy consistent entrainment model for volumetrically forced jets using large eddy simulations. *Phys. Fluids* 30: 105107
- [27] Bhattacharya A and Pant C S 2017 Validation of a one dimensional model for volumetrically forced jets using large eddy simulations. *APS KPI*–129
- [28] Agrawal A, Sreenivas K R, and Prasad A K 2004 Velocity and temperature measurements in an axisymmetric turbulent jet with cloud-like off-source heating. *Int. J. Heat Mass Transf.* 47: 1433–1444
- [29] Bhat G S and Narasimha R 1996 A volumetrically heated jet: large-eddy structure and entrainment characteristics. *J. Fluid Mech.* 325: 303–330
- [30] Pant C S and Bhattacharya A 2016 A viscous sponge layer formulation for robust large eddy simulation of thermal plumes. *Comput. Fluids* 134: 177–1896
- [31] Pant C S and Bhattacharya A 2017 Application of sponge boundary conditions to large-eddy simulation of multiple thermal plumes. In *Progress in Turbulence VII*, Springer: 239–244
- [32] Diwan S S, Ravichandran S, Govindarajan R, and Narasimha R 2020 Understanding transmission dynamics of covid-19-type infections by direct numerical simulations of cough/sneeze flows. *Trans. Indian Natl. Acad. Eng.* 1
- [33] Lehmann K, Siebert H, and Shaw R A 2009 Homogeneous and inhomogeneous mixing in cumulus clouds: dependence on local turbulence structure. *J. Atmos. Sci.* 66: 3641–3659
- [34] Kumar B, Schumacher J, and Shaw R A 2014 Lagrangian mixing dynamics at the cloudy–clear air interface. *J. Atmos. Sci.* 71: 2564–2580
- [35] Srivastava A 2020 Covid-19 and air pollution and meteorology—an intricate relationship: a review. *Chemosphere* 128297
- [36] Agrawal A and Bhardwaj R 2020 Reducing chances of covid-19 infection by a cough cloud in a closed space. *Phys. Fluids* 32: 101704
- [37] Dbouk T and Drikakis D 2020 On coughing and airborne droplet transmission to humans. *Phys. Fluids* 32(5): 053310
- [38] <https://grabcad.com/library/male-face>; accessed 11 September, 2020
- [39] Pant C S and Bhattacharya A 2015 The effect of initial droplet size spectra on its evolution during turbulent condensational growth. *Proc. IUTAM* 15: 41–48
- [40] Pinsky M, Khain A, and Korolev A 2016 Theoretical analysis of mixing in liquid clouds—part 3: inhomogeneous mixing. *Atmos. Chem. Phys. (Online)* 16: 9273–9297
- [41] Arumuru V, Pasa J, and Samantaray S S 2020 Experimental visualization of sneezing and efficacy of face masks and shields. *Phys. Fluids* 32: 115129
- [42] <https://www.accuweather.com>; accessed 05 May, 2020

- [43] Lasher-trapp S G, Cooper W A, and Blyth A M 2005 Broadening of droplet size distributions from entrainment and mixing in a cumulus cloud. *Quart. J. Roy. Meteorol. Soc. J. Atmos. Sci. Appl. Meteorol. Phys. Oceanogr.* 131: 195–220
- [44] Segal Y, Pinsky M, Khain A , and Erlick C 2003 Thermodynamic factors influencing bimodal spectrum formation in cumulus clouds. *Atmos. Res.* 66: 43–64